https://doi.org/10.5194/egusphere-2023-777
Preprint. Discussion started: 3 May 2023

BVOC emission flux response to the El Niño-Southern Oscillation

Ryan Vella[1,2], Andrea Pozzer[1,4], Matthew Forrest[3], Jos Lelieveld[1,4], Thomas Hickler[3,5], and Holger Tost[2]

[1]Atmospheric Chemistry Department, Max Planck Institute for Chemistry, Mainz, Germany
[2]Institute for Atmospheric Physics, Johannes Gutenberg University Mainz, Mainz, Germany
[3]Senckenberg Biodiversity and Climate Research Centre (SBiK-F), Frankfurt am Main, Germany
[4]Climate and Atmosphere Research Center, The Cyprus Institute, Nicosia, Cyprus
[5]Department of Physical Geography, Goethe University, Frankfurt am Main, Germany

Correspondence: Ryan Vella (ryan.vella@mpic.de)

Abstract.

Isoprene and monoterpene emissions from the terrestrial biosphere play a significant role in major atmospheric processes. Emissions depend on the vegetation's response to atmospheric conditions (primarily temperature and light), as well as other stresses e.g. from droughts and herbivory. It has been well documented that biogenic volatile organic compound (BVOC) emissions are sensitive to climatic influences. The El Niño-Southern Oscillation (ENSO) is a natural cycle, arising from sea surface temperature (SST) anomalies in the tropical Pacific, which perturbs the natural seasonality of weather systems on both global and regional scales. Several studies evaluated the sensitivity of BVOC fluxes during ENSO events using historical transient simulations. While this approach employs realistic scenarios, it is difficult to assess the individual impact of ENSO given multiple forcing on the climate system e.g. from anthropogenic emissions of CO_2 and aerosol. In this study, a global atmospheric chemistry-climate model with enabled interactive vegetation was used to conduct two sets of simulations: 1) isolated ENSO event simulations, in which a single ENSO event is used to perturb otherwise baseline conditions, and 2) sustained ENSO simulations, in which the same ENSO conditions are reproduced for an extended period of time. From the isolated ENSO events, we present global and regional BVOC emission changes resulting from the immediate vegetation response to atmospheric states. More focus is given to the sustained ENSO simulations which have the benefit of reducing the internal variability for more robust statistics when linking atmospheric and vegetation variables with BVOC flux anomalies. Additionally, these simulations explore long-term changes in the biosphere with potential shifts in vegetation in this possible climate mode, accounting for the prospect of increased intensity and frequency of ENSO with climate change. Our results show that strong El Niño events increase global isoprene emission fluxes by 2.9% and that one single ENSO event perturbs the Earth system to the point where BVOC emission fluxes do not return to baseline emissions within several years after the event. We show that persistent ENSO conditions shift the vegetation to a new quasi-equilibrium state, leading to an amplification of BVOC emission changes with up to 19% increase in isoprene fluxes over the Amazon. We provide evidence that BVOC-induced changes in plant phenology such as the leaf area index (LAI), have a significant influence on BVOC emissions in the sustained ENSO climate mode.

https://doi.org/10.5194/egusphere-2023-777
Preprint. Discussion started: 3 May 2023

1 Introduction

The terrestrial biosphere is a major source of natural volatile organic compounds (VOCs), such as isoprene and monoterpenes, accounting for approximately 90% of all VOC emissions to the atmosphere (Guenther et al., 1995). Isoprene and monoterpenes are thought to work against stress-induced reactive oxygen species or help plants coping with abiotic stress by changing membrane properties (Sharkey and Loreto, 1993; Vickers et al., 2009; Karl et al., 2010; Sharkey and Monson, 2017), while they can also be induced by other chemical, physical, or biological processes, such as herbivory (Laothawornkitkul et al., 2008) and signaling between organisms (Zuo et al., 2019). Biogenic volatile organic compounds (BVOCs) are highly reactive and short-lived (minutes to hours) as they quickly interact with tropospheric oxydant gases upon emission, exerting a significant influence on the atmosphere's oxidation capacity (Atkinson, 2000; Atkinson and Arey, 2003). The dominant reaction mechanism is OH oxidation, which has significant implications for secondary organic aerosol formation, and in turn, for cloud formation and climate (Pöschl et al., 2010; Ehn et al., 2014; Palm et al., 2018). OH oxidation of BVOCs has also implications on greenhouse gas and pollutant concentrations (e.g. methane and CO; Arneth et al., 2010; Peñuelas and Staudt, 2010).

The El Niño-Southern Oscillation (ENSO) is the periodic oscillation (occurring every 2 to 7 years) between anomalously warm (El Niño) and cold (La Niña) sea surface temperatures (SSTs) in the tropical Pacific (McPhaden et al., 2006). Because of the strong interactions between atmospheric and oceanic circulations, such anomalies in tropical Pacific SST have a significant impact on atmospheric processes. ENSO therefore exerts substantial influence on weather systems and global climate patterns (McPhaden et al., 2006). During ENSO events, the Walker circulation convective centers re-arrange, inducing precipitation anomalies in the tropics as well as influencing monsoon systems via the Hadley circulation over the Pacific, Indian, and Atlantic Oceans. Teleconnections with midlatitude westerlies can also result in consistent anomaly patterns in the extratropics (Dai and Wigley, 2000). To this end, tropical regions during El Niño episodes are often much warmer and drier than average (Gong and Wang, 1999; Dai and Wigley, 2000) but some regions tend to be cooler and wetter, e.g., western North America (Ropelewski and Halpert, 1986) and East Asia (Wu et al., 2003).

Several studies explored the sensitivity of the terrestrial biosphere to different ENSO phases (e.g., Ahlström et al., 2015; Chang et al., 2017; Bastos et al., 2018; Teckentrup et al., 2021). The primary factors driving changes in vegetation are closely linked to the dominant meteorological drivers of net primary productivity (NPP) in different regions. Specifically, radiation is the primary driver in wet tropics, moisture in dry tropics and temperate regions, and temperature in the western temperate and boreal regions (Nemani et al., 2003). The terrestrial biosphere often acts as a carbon source during El Niño events, while carbon uptake increases during La Niña events, particularly in semi-arid ecosystems (Ahlström et al., 2015). Nevertheless, the complex relationships between ENSO-induced climatic variability and terrestrial ecosystem productivity, particularly the extent, amplitude, and underlying processes, remain poorly understood (Gonsamo et al., 2016; Wang et al., 2018; Zhu et al., 2017). Zhang et al. (2019) linked ENSO seasonality with global gross primary production (GPP) and found peak correlations occurring between global yearly GPP and ENSO conditions in August and October of the preceding year. Isoprene emissions based on satellite formaldehyde (HCHO) measurements also show interannual differences tied to temperature shifts and climate features such as El Niño (Wells et al., 2020). Modelling studies have suggested that BVOC emissions are generally higher

https://doi.org/10.5194/egusphere-2023-777
Preprint. Discussion started: 3 May 2023

during El Niño years and lower during La Niña years, with ENSO having a significant impact in both the Tropics and the higher latitudes (Lathiere et al., 2006; Müller et al., 2008).

In this study, sea surface temperatures (SSTs) and sea ice cover (SICs) associated with ENSO years are used to construct different ENSO scenarios: very strong and moderate El Niño / La Niña scenarios as well as a baseline scenario. An Earth System Model (ESM) with interactive vegetation representations is used to investigate ENSO-induced changes in meteorology, vegetation, and BVOC emissions on global and regional scales. We present two sets of simulations: (1) isolated ENSO event simulations, which employ a single ENSO event in otherwise baseline conditions, and (2) sustained ENSO simulations, which use the same ENSO conditions over a 30-year period. Both sets of simulations are used to evaluate the various effects of ENSO. The isolated ENSO event simulations are used to study the temporal evolution of BVOC anomalies following a single ENSO event and to estimate global and regional changes resulting from the immediate response of the biosphere to atmospheric states anomalies. The most recent IPCC assessment based on CMIP6 simulations states that ENSO will continue to be the primary mode of interannual variability in a warmer climate, with a high degree of certainty (Lee et al., 2021). However several studies have suggested the possibility of more persistent ENSO conditions in the future (e.g. Bacer et al., 2016; Cai et al., 2015). Here, we us the sustained ENSO simulations to explore the upper range of impacts of ENSO, as well as long-term changes in the biosphere and the resulting BVOC emission fluxes in this such a climate mode.

2 Methods

2.1 Models

The EMAC modelling system

The EMAC (ECHAM/MESSy Atmospheric Chemistry) model is a numerical chemistry and climate modelling system that contains submodels that represent tropospheric and middle atmospheric processes, as well as their interactions with oceans, land, and anthropogenic activities. It originally combined the ECHAM atmospheric GCM (Roeckner et al., 2006) with the Modular Earth Submodel System (MESSy) (Jöckel et al., 2005) framework and philosophy where physical processes and most of the infrastructure has been modularized into submodels that can be further developed to improve existing process representations and new submodels can be added to represent new or alternative process representations. In recent years EMAC has been further developed to include a broader representation of atmospheric chemistry by coupling different processes such as representations for aerosols, aerosol–radiation and aerosol–cloud interactions, e.g. Tost (2017). In this study, the version 2.55 has been utilised, which is based on the well documented version used in comprehensive model intercomparison studies, e.g., Jöckel et al. (2016).

LPJ-GUESS

The following section is based on the standard copyright-free LPJ-GUESS model description template (https://web.nateko.lu.se/lpj-guess/resources.html,last access: 21 December 2022). Lund-Potsdam-Jena General Ecosystem Simulator (LPJ-GUESS) (Smith et al., 2001, 2014) is a dynamic global vegetation model (DGVM) featuring an individual-based model of vegetation dynamics. These dynamics are simulated as the emergent outcome of growth and competition for light, space and soil resources

https://doi.org/10.5194/egusphere-2023-777
Preprint. Discussion started: 3 May 2023

among woody plant individuals and a herbaceous understorey in each of a number (50 in this study) of replicate patches representing random samples of each simulated locality or grid cell. The simulated plants are classified into twelve plant functional types (PFTs) discriminated by growth form, phenology, photosynthetic pathway (C3 or C4), bioclimatic limits for establishment and survival and, for woody PFTs, allometry and life history strategy. LPJ-GUESS has previously been implemented in global ESMs (e.g. Weiss et al., 2014; Alessandri et al., 2017), and more recently coupled with EMAC (Forrest et al., 2020; Vella et al., 2023). The LPJ-GUESS version used in this study currently provides information on potential natural vegetation rather than present-day vegetation and does not implement land use changes.

2.2 EMAC-LPJ-GUESS configuration

In this study, the standard EMAC-LPJ-GUESS coupled configuration (as presented in Forrest et al., 2020; Vella et al., 2023) is used, where the vegetation in LPJ-GUESS is entirely determined by the EMAC atmospheric state, soil, N deposition, and fluxes while the BVOC modules in EMAC run on dynamic vegetation information (LAI, foliar density, leaf area density distribution, and PFT fractional coverage) from LPJ-GUESS. The BVOC emission modules in EMAC are ONEMIS (Kerkweg et al., 2006) and MEGAN (Guenther et al., 2006) and are both based on the Guenther algorithms (Guenther et al., 1993, 1995). Refer to Vella et al. (2023) for coupling details. In this work, BVOC fluxes from ONEMIS are evaluated, where emissions are calculated as a function to ecosystem specific emission factors, surface radiation, temperature, the foliar density and its vertical distribution.

2.3 Experimental design

A thirty-year (1980-2009) AMIPII SST & SIC dataset (https://pcmdi.llnl.gov/mips/amip/amip2/, last access: 12 January 2023) was used to evaluate the Oceanic Niño Index (ONI) and classify the strength of different ENSO events. Running 3-month mean SST anomalies in the Niño 3.4 region (5°N-5°S, 120°-170°W), based on this 30-year base period, are shown in the top panel of Fig. 1. Events are defined when the anomaly is greater or equal to $0.5°$ for five consecutive overlapping 3-month periods ($+0.5°$ for El Niño events and $-0.5°$ for La Niña events). Furthermore, events are categorised into *Weak* (0.5 to 0.9 SST anomaly), *Moderate* (1.0 to 1.4), *Strong* (1.5 to 1.9) or *Very Strong* (≥ 2.0) when the threshold is reached or exceeded for at least three consecutive overlapping 3-month periods.

https://doi.org/10.5194/egusphere-2023-777
Preprint. Discussion started: 3 May 2023

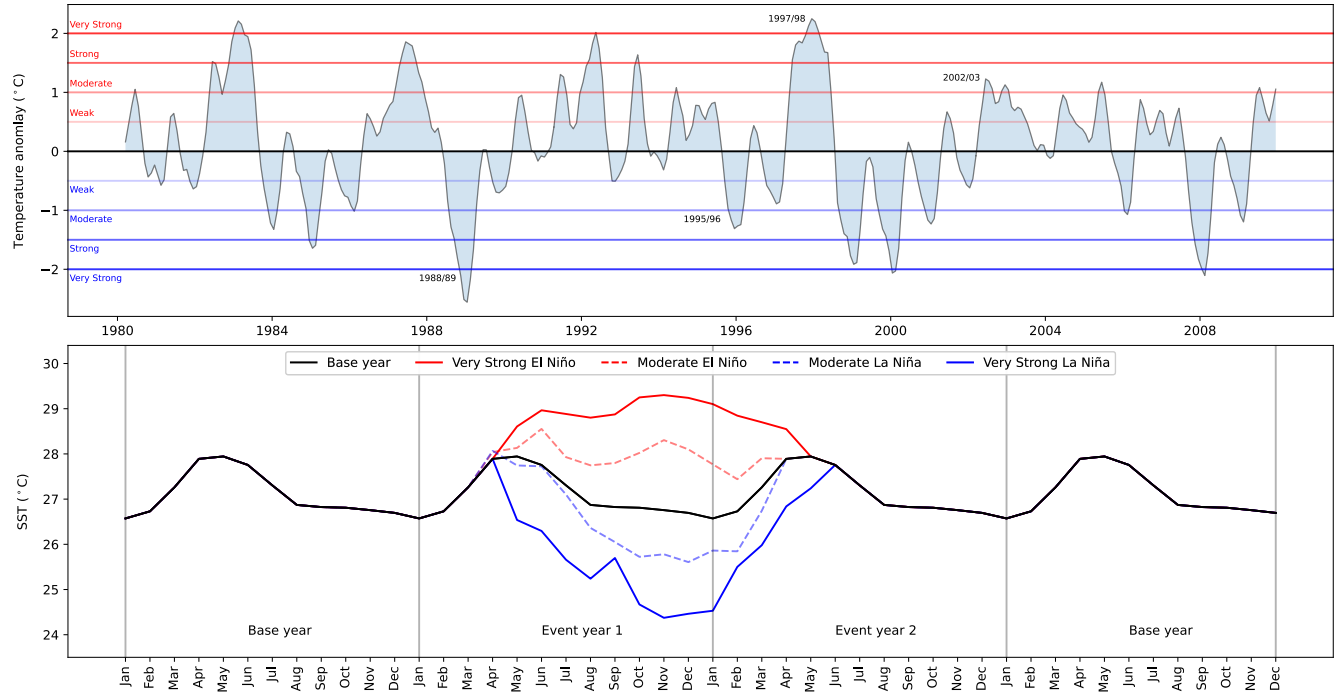

Figure 1. Top panel: SST anomaly in Niño 3.4 region from 1980 to 2009. Horizontal lines indicate the anomaly strength (El Niño in red & La Niña in blue). Dates of notable ENSO events used in this study are marked. Bottom panel: Four consecutive years of SST in Niño 3.4 region. The two years in the middle indicate four ENSO scenarios as well as the base scenario.

Global SST and SIC are used as forcing data to construct four scenarios: (1) Very Strong El Niño (based on 1997/98); (2) Moderate El Niño (based on 2002/03); (3) Very Strong La Niña (based on 1988/89); and (4) Moderate La Niña (based on 1995/96). The event typically spans from March to June of the following year. The lower panel of Fig. 1 shows SST values in the El Niño 3.4 region. The base year (i.e. the 30-year average SST over El Niño 3.4) is shown in black while the ENSO events are shown in red (El Niño) and blue (La Niña). During ENSO events, SST starts to deviate from baseline conditions in March/April of the first event year and continues until April/May/June of the following year (event year 2). This study looks at atmospheric, vegetational and BVOC emission changes in sustained ENSO scenarios with continuous ENSO forcing, as well as the temporal evolution of BVOC emissions following an isolated event under otherwise baseline conditions. To do so, two sets of global simulations, hereinafter referred to as *sustained* and *isolated* simulations, are performed. Both sets of simulations run at a horizontal resolution of T63 (approximately $1.9° \times 1.9°$ at the Equator) and have a 500-year offline spin-up phase. In this work, we focus especially on seven regions, defined in the supplement material and also presented graphically in Fig. 4, 5, and 7. Given the regional nature of BVOC emission changes from ENSO, the areas were chosen based upon roughly consistent BVOC anomalies in areas with high emission rates i.e. mostly in the tropics.

https://doi.org/10.5194/egusphere-2023-777
Preprint. Discussion started: 3 May 2023

Isolated ENSO event simulations

This simulation setup is designed to trigger a single ENSO event (spread over two years) in otherwise baseline conditions. The evolution (with respect to time) of the SST temporal simulations is depicted in the lower panel of Fig. 1. The simulations used *base* conditions for the whole simulation time except for the two event years, where a perturbation in the SST and SIC is introduced according to the specific ENSO event considered. The 50-year simulations run with *base* conditions all the time except for the 31st and 32nd year of the simulation. The events considered with this setup are *very strong* La Niña event (based on SST and SIC from May to December 1988 and January to April 1989), and *very strong* El Niño event (based on SST and SIC from May to December 1997 and January to March 1998). With this setup, temporal variations in BVOC emissions during *very strong* ENSO events and in subsequent years can be assessed. These simulations differ from previous studies, where BVOC emission changes due to ENSO are typically evaluated using satellite data (e.g. Zhang et al., 2019; Wells et al., 2020) or with transient (i.e historical) simulations (e.g. Bastos et al., 2018; Teckentrup et al., 2021). The advantage of the isolated ENSO simulations implemented in the constant climate boundary conditions (i.e. SSTs and SICs), and therefore the changes in BVOC fluxes presented here are purely coming from ENSO and not other climatic forcing (e.g. due to trends from CO_2, aerosol loading, etc.) which may influence a transient simulation.

Sustained ENSO simulations

Event though the isolated ENSO simulations give realistic insights on changes in BVOC fluxes with respect to the magnitude and time evolution, it is hard to constrain ENSO-induced changes statistically from a single simulation run given the high internal variability within the system. We therefore further analysed model results from sustained ENSO simulations. These simulations provide persistent ENSO conditions over many years by prescribing the same yearly cycle of SST and SIC data over thirty simulated years. The five scenarios employ the following global SST and SIC data: (1) *base* simulation - monthly average SST and SIC from 1980 to 2009 (30 years); (2) *moderate* El Niño - April to December 2002 and January to March 2003; (3) *very strong* El Niño - May to December 1997 and January to March 1998; (4) *moderate* La Niña scenario - April to December 1995 and January to March 1996; and (5) *very strong* La Niña scenario - May to December 1988 and January to April 1989. The corresponding SSTs used in these simulations can be seen in the bottom panel of Fig. 1. The base simulation uses SSTs from Jan to Dec, while the ENSO simulations use different 12-month frames between Event year 1 and 2. In the later simulations, the monthly order of the months may be disrupted, meaning that month 1 in the simulation could be March, April, or May, instead of January. However, the yearly ENSO cycle is still conserved, and since the same monthly SST and SIC data are used for every year of the simulations, the specific order of the months does not affect the results.

These simulations constrain better the correlations between BVOC flux emissions, meteorology and vegetation changes and they provide statistical confidence that the characterised perturbations are caused by ENSO rather than other variability attributed to the climate system. However, we emphasise that these simulations express ENSO scenarios where the vegetation comes into quasi-equilibrium with the new climate system. The reported BVOC emissions changes are therefore exaggerated as they include drifts in the vegetation states resulting from years to decades of plant establishment and mortality. Nonetheless, given the possible intensification of ENSO with climate change (Bacer et al., 2016; Cai et al., 2015) these simulations provide insights on possible vegetation changes and the subsequent effects on BVOC emission fluxes.

https://doi.org/10.5194/egusphere-2023-777
Preprint. Discussion started: 3 May 2023

Simulation Name	Simulation Type	Details
Base Very Strong El Niño Very Strong La Niña	Isolated ENSO simulations	T63 horizontal resolution. 500-year offline spin-up phase. 40 years long, using the last 11 years for analysis. Base global SST & SIC conditions except for the "event" years on the 31st / 32nd year of the simulation.
Base Very Strong El Niño Moderate El Niño Very Strong La Niña Moderate La Niña	Sustained ENSO simulations	T63 horizontal resolution. 500-year offline spin-up phase. 50 years long, using the last 30 years for analysis. Same conditions applied in every year of the simulation.

Table 1. Summary of the simulations carried out in this study.

3 Results and Discussion

3.1 Isolated ENSO events simulations

This section presents results from the isolated simulations described in Section 2.3. Fig. 2 shows 12-month moving averages of monthly isoprene emissions globally and over seven regions (see Table 1 in supplement material). The event, spanning over two years, is marked in green while the following two years are marked in yellow. Isoprene fluxes from El Niño, La Niña, and Base conditions are shown in red, blue and black, respectively. Notice that prior to the event, the isoprene fluxes in all cases are identical, however, the ENSO perturbation from the respective event makes the fluxes diverge from each other. The anomalies in BVOC emission fluxes result from the immediate response of vegetation due to changes in meteorological states brought by ENSO. The changes noted here can also be solely attributed to Pacific SST anomalies and not other forcing within the Earth system.

https://doi.org/10.5194/egusphere-2023-777
Preprint. Discussion started: 3 May 2023

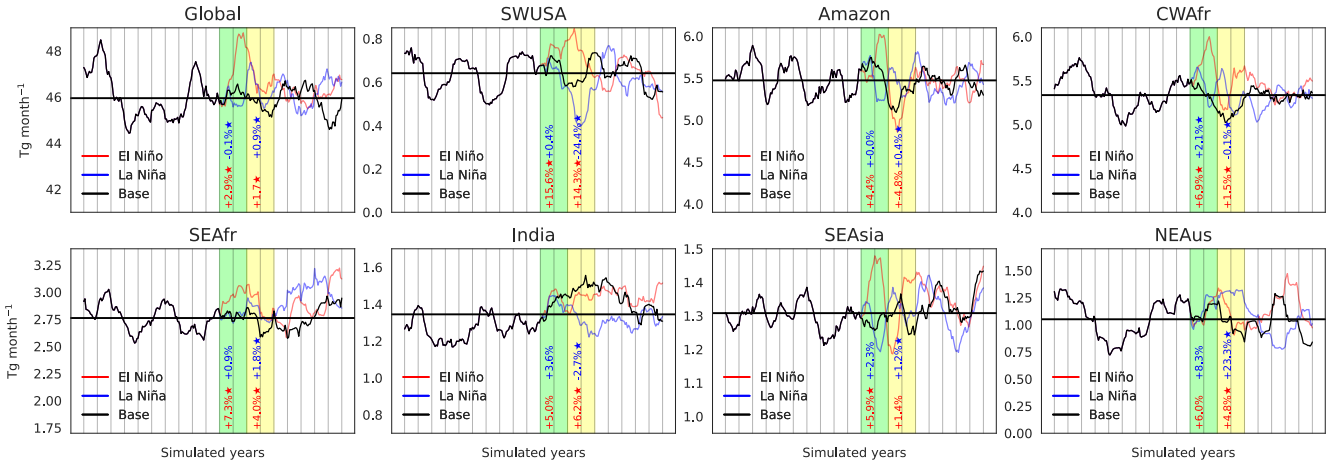

Figure 2. Time evolution of global and regional isoprene fluxes with El Niño (red) and La Niña (blue) events over two years (green columns). The black line illustrates the mean over base conditions throughout all simulation. Vertical grey lines correspond to simulated years. Only 10 of the 30 simulated years before the ENSO event are shown. Statistically significant changes (p<.01) are marked with a star.

Fig. 2 includes percentage changes of El Niño (in red) and La Niña (in blue) fluxes compared to the *base* simulation during the event (in green) and the subsequent two years (in yellow). The percentage changes include a star symbol when the difference from the base emissions is statistically significant (99% confidence with a two-tailed Student's t-test i.e. $p < .01$), over that time-frame. Global isoprene emissions increase by 2.9% during an El Niño and remain elevated by 1.7% in the two years following the event. During El Niño and the subsequent two years, SWUSA experiences a rise of 15.6% and 14.3%, respectively, while a decline of 24.4% is found in SWUSA during the two years following La Niña. Other notable emission changes occur in CWAfr, SEAfr and SEAsia for the El Niño event. A significant increase of 23.3% in the two years following La Niña in NEAus is also present. Our results suggest that changes in isoprene fluxes due to an ENSO event are very regional and, on a global scale, higher emissions during and following a strong El Niño event are present. These findings agree with previous studies suggesting that high BVOC emissions are often associated to El Niño years (e.g. 1997/1998), and low emissions to La Niña years (e.g. 1995/1996) (e.g Lathiere et al., 2006; Müller et al., 2008). These simulations also show that the perturbation introduced by the ENSO event stretches for a long time following the event, even though the SST and SIC are restored to *base* conditions. Monoterpene emissions follow similar changes as isoprene fluxes with a global increase of 3.2% during an El Niño event (see Fig. S2 in the supplement).

In order to attribute the changes in isoprene emissions, we look into correlations between the standardized isoprene flux anomalies and the temperature, radiation, aridity index (AI), net primary production (NPP) and, leaf area index (LAI) standardized anomalies during the event years and the following 2 years (total of 4 years) from the isolated ENSO simulations. The AI is defined as the total precipitation divided by the potential evaporation/sublimation (including evapotranspiration (PET)). The standardized anomaly is calculated by dividing the anomalies by the standard deviation of the base scenario. Fig. 3 shows

https://doi.org/10.5194/egusphere-2023-777
Preprint. Discussion started: 3 May 2023

such correlations for El Niño (top panels) and La Niña (bottom panels). The r values for each region is shown and correlations with $p < .01$ are marked with a start sign.

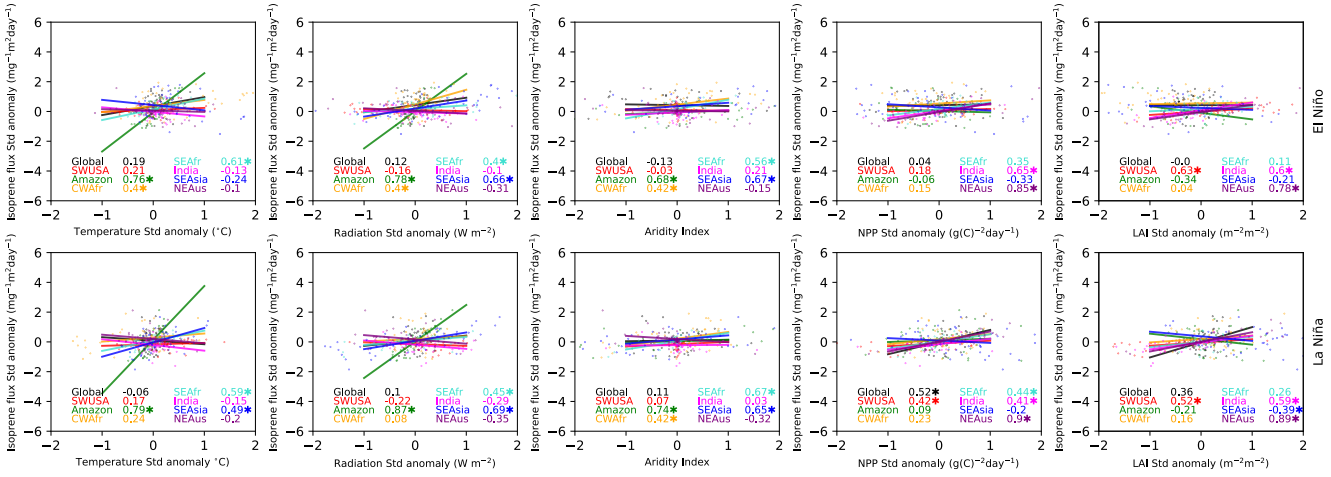

Figure 3. The Person's correlation (r) between the standardized isoprene flux anomaly and standardized temperature, radiation, AI, NPP, and LAI anomaly at different regions for the event years and the following two years (four years in total). Very strong El Niño and La Niña events are shown in the top and bottom panels, respectively.

We note that the dependencies in isoprene emissions are very region-specific, so much so that correlations on a global scale are generally very poor. For the El Niño event, the standardized isoprene anomaly correlates strongly with the standardized temperature, radiation, and AI anomaly over the Amazon, and SEAsia. Strong dependencies on NPP occur over India and NEAus, while dependencies on LAI are significant over SWUSA, India, and NEAus. Similar dependecies are seen during La Niña with very high correlation with vegetation variables (NPP and LAI) over NEAus. While over SWUSA, India, SEAsia, and NEAus, isoprene anomalies correlate very well with vegetation changes, emission anomalies over the Amazon, CWAfr, and SEAfr mostly depend on changes in surface temperature and radiation. Monoterpene fluxes exhibit similar dependencies (figure included in supplement material).

3.2 Sustained ENSO simulations

The isolated ENSO simulations discussed so far give insights on the temporal evolution of BVOC emission changes from single ENSO events. Here we present results from sustained ENSO conditions based on the last thirty ensemble years from 50-year simulations at a horizontal resolution of T63 with a 500-year offline spin-up phase. These simulations have the advantage of minimising the influence of internal variability and thus enhancing potential links between ENSO, meteorology, vegetation and BVOC emission fluxes. This climatic mode, albeit not realistic at present, is possible with the intensification of ENSO with climate change, and allows us to study long-term effects on the biosphere and BVOC emission fluxes.

https://doi.org/10.5194/egusphere-2023-777
Preprint. Discussion started: 3 May 2023

3.2.1 Changes in atmospheric drivers during ENSO

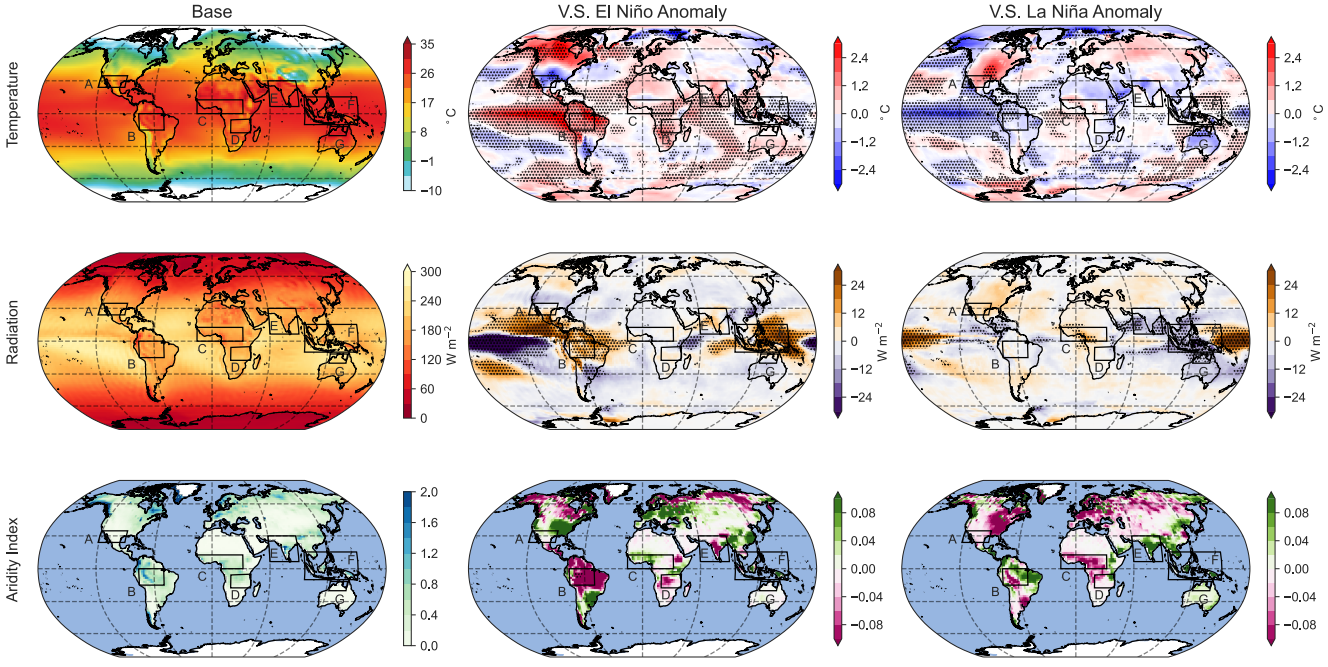

Figure 4. Global distribution of surface temperature, solar radiation, and AI during the base scenario (left panels) averaged over 30 years. The middle panels show El Niño anomalies and the right panels show LA Niña anomalies. Areas with statistically significant anomalies ($p <$ .01) are marked with black dots.

Fig. 4 shows global distributions of surface temperature, net solar radiative flux at the surface, and the AI averaged over 30 years for the base scenario as well as anomalies from very strong El Niño and La Niña scenarios. Table 2 shows the percentage changes in surface temperature, radiation and AI during the ENSO conditions compared to the base scenario, globally, and the indicated areas of interest. Statistically significant anomalies ($p < .01$) are shown in green.

El Niño generally results in positive temperature anomalies, with statistically significant positive anomalies occurring over the Amazon (+ 5.84%), CW Africa (+ 1.95%), SE Africa (+ 2.80%), and SE Asia (+ 0.30%). During La Niña, the only significant negative temperature anomalies occur over the Amazon (-1.49%) and CW Africa (-1.44%).

https://doi.org/10.5194/egusphere-2023-777
Preprint. Discussion started: 3 May 2023

	El Niño (% Diff)			La Niña (% Diff)		
Area	Temp (°C)	Rad	AI	Temp (°C)	Rad	AI
Global	3.85 (0.25°)	−0.13	3.24	−1.54 (−0.1°)	0.21	44.27
SWUSA	−2.66 (−0.55°)	58.5	13.36	2.80 (0.58°)	2.83	−47.5
Amazon	5.84 (1.51°)	6.03	−27.49	−1.49 (−0.39°)	−0.12	0.34
CWAfr	1.95 (0.54°)	1.79	−19.27	−1.44 (−0.4°)	1.22	17.1
SEAfr	2.80 (0.65°)	0.03	−3.17	−1.21 (−0.28°)	−0.82	0.69
India	1.96 (0.52°)	1.09	−26.02	−0.88 (−0.23°)	−3.72	31.95
SEAsia	0.30 (0.09°)	7.25	0.71	0.05 (0.01°)	−1.5	32.87
NEAus	0.38 (0.11°)	−0.14	2.55	−2.09 (−0.62°)	−3.57	83.71

Table 2. Percentage changes in temperature, radiation and the aridity index (AI) for El Niño and La Niña scenarios. Statistically significant anomalies ($p < .01$) are highlighted in green.

During El Niño, significant positive surface radiation anomalies occur over the Amazon (+ 6.03%), and SE Asia (+7.25%), while La Niña results in significant positive radiation anomalies over CWAfr (1.22) and negative anomalies over India (−3.72%), SEAsia (−1.5) and NEAus (−3.57%). AI anomalies are not statistically significant but suggest that the Amazon, CWAfr and India become considerably dryer during El Niño while India, SEASIA, and NEAus wetter during La Niña. Overall, both El Niño and La Niña lead to substantial regional modulations of the key meteorological variables without disturbing the global energy and water budgets.

3.2.2 Vegetation response

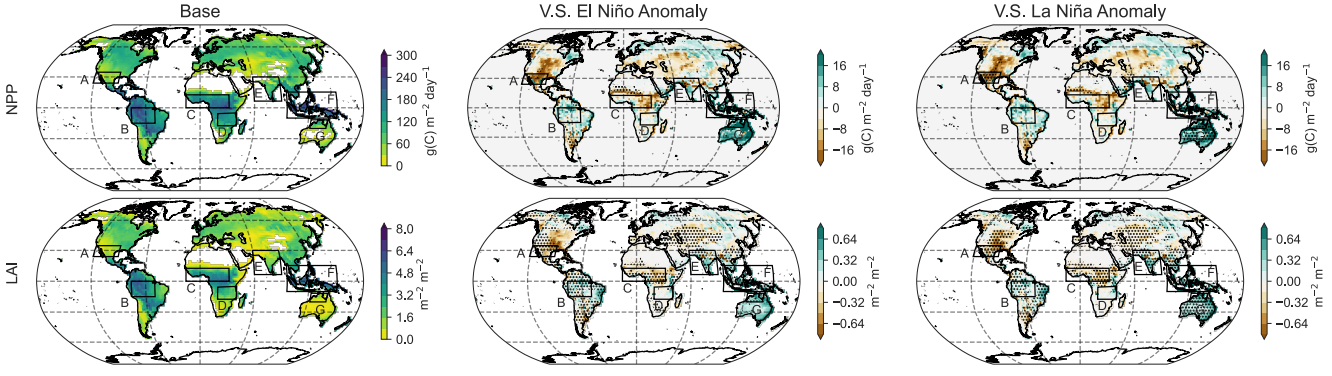

Figure 5. Distribution of NPP and LAI for base conditions (left panels) and anomalies in very strong El Niño (middle panels) and very strong La Niña (right panels).

https://doi.org/10.5194/egusphere-2023-777
Preprint. Discussion started: 3 May 2023

	El Niño (% Diff)		La Niña (% Diff)	
Area	NPP	LAI	NPP	LAI
Global	0.61	−2.99	1.25	2.91
SWUSA	15.49	23.53	−23.93	−32.58
Amazon	−2.06	−7.19	1.79	2.20
CWAfr	−4.28	−11.99	2.88	4.76
SEAfr	2.56	1.32	0.04	2.81
India	−1.57	−5.14	−3.96	11.46
SEAsia	−11.78	−23.42	9.89	17.01
NEAus	13.29	14.02	44.39	78.43

Table 3. Percentage changes in NPP and LAI for El Niño and La Niña scenarios. Statistically significant anomalies ($p < .01$) are highlighted in green.

The model configuration used in this study links atmospheric states with vegetation dynamics. Given that the vegetation is responsive to temperature, solar radiation, and soil moisture, changes in atmospheric states during an ENSO event also modify the state of the vegetation. Fig 5. shows the distribution of the net primary production (NPP) and leaf area index (LAI) during the base case as well as anomalies in the same parameters during El Niño and La Niña scenarios. Percentage changes in the NPP and LAI are presented in Table 3. During El Niño, the NPP only changes significantly over SE Asia (-11.78%). The global LAI decreases by almost 3%, while regionally, the LAI increases over SWUSA (+ 23.53%) and decreases over the Amazon (-7.19%), CWAfr (-11.99%), and SEAsia (-23.42%), during El Niño. La Niña results in a decrease in NPP over SWUSA (-23.93%), and an increase over SEAsia (+ 9.89%) and NEAus (+ 44.39%). During La Niña the global LAI increases significantly by 2.91%, while regionally the LAI decreases over SWUSA (-32.58%), and increases over the Amazon (+ 2.20%), CWAfr (+ 4.76%), India (+ 11.46%), SEAsia (+ 17.01%), and NEAus (+ 78.43%). The LAI is mostly linked to water stresses and and matches changes in the AI, see Table 2.

The biosphere responds on different time scales to atmospheric changes: while the NPP responds nearly instantaneously, the LAI responds rather quickly (within 1 year), but changes in vegetation fractions are very slow as they result from years to decades of plant establishment and mortality. With the intensification of ENSO, we could be moving towards a new quasi-equilibrium state where the vegetation states adapt to the new climate. Fig. 6 shows changes in the vegetational fractional coverage of the dominant PFTs over SWUSA, Amazon, SEAsia, and India at the different scenarios in this climate mode.

https://doi.org/10.5194/egusphere-2023-777
Preprint. Discussion started: 3 May 2023

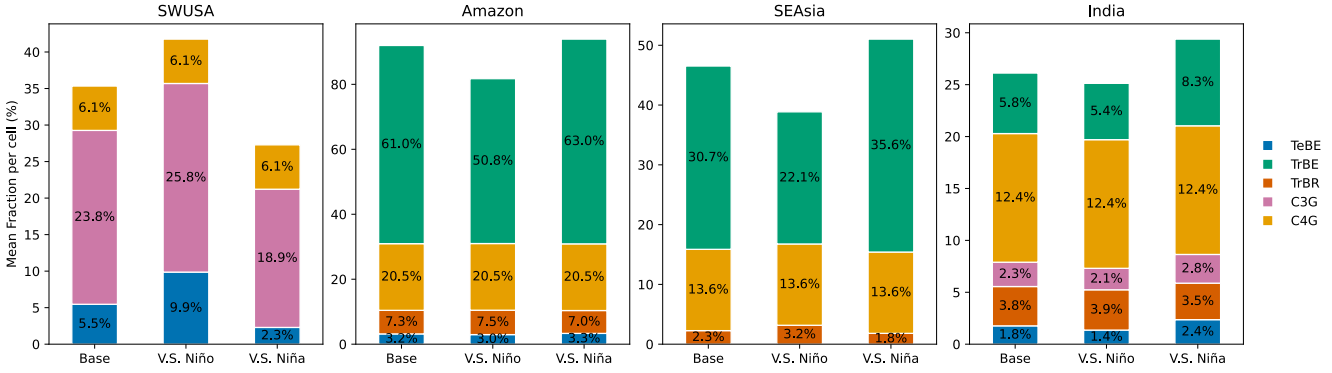

Figure 6. Stacked bar plots for the fractional coverage (% of the total area) per PFT during the base case, VS El Niño, and VS La Niña scenarios over the USA, Amazon, Asia, and India. Only PFTs with a fractional coverage higher than 1% are shown. The PFTs shown are: temperate broad-leaved evergreen trees (TeBE), tropical broad-leaved evergreen trees (TrBE), tropical broad-leaved rain-green trees (TrBR), cool C3 grass (C3G), and warm C4 grass (C4G).

The SWUSA is a semi-arid region dominated by grass but also includes temperate broad-leaved evergreen trees (TeBE). Compared to the base case, the SWUSA sees an increase in vegetational coverage during El Niño. The area covered by TeBe grows by 2%, and warm C4 grass (C4G) by 4.4%. Conversely, during La Niña, TeBe and C4G shrinks by 4.9% and 3.4%, respectively. In comparison to the base case, the SWUSA experiences an increase in vegetation during El Niño. TeBe's area coverage expands by 2%, and warm C4 grass (C4G) increases by 4.%. On the other hand, during La Niña, both TeBe and C4G diminish by 4.9% and 3.4%, respectively. Over the Amazon, there are also notable changes in PFT coverage especially in the El Niño scenario, where tropical broad-leaved trees (TrBE) decrease by 10.2%. On the other hand, TrBE increases by 2% during La Niña. Over SEAsia, during El Niño TrBE decreases by 8.6% during El Niño and increase 4.9% during La Niña. The area over India consists of more PFTs and changes compared to the base case mostly occur in the La Niña scenario where the fractional coverage of TrBE increases by 2.5%. Over CWAfr, SEAfr, NEAus, and globally, changes in fractional coverage of different PFTs during the ENSO events were found to be negligible.

https://doi.org/10.5194/egusphere-2023-777
Preprint. Discussion started: 3 May 2023

3.2.3 BVOC emission changes

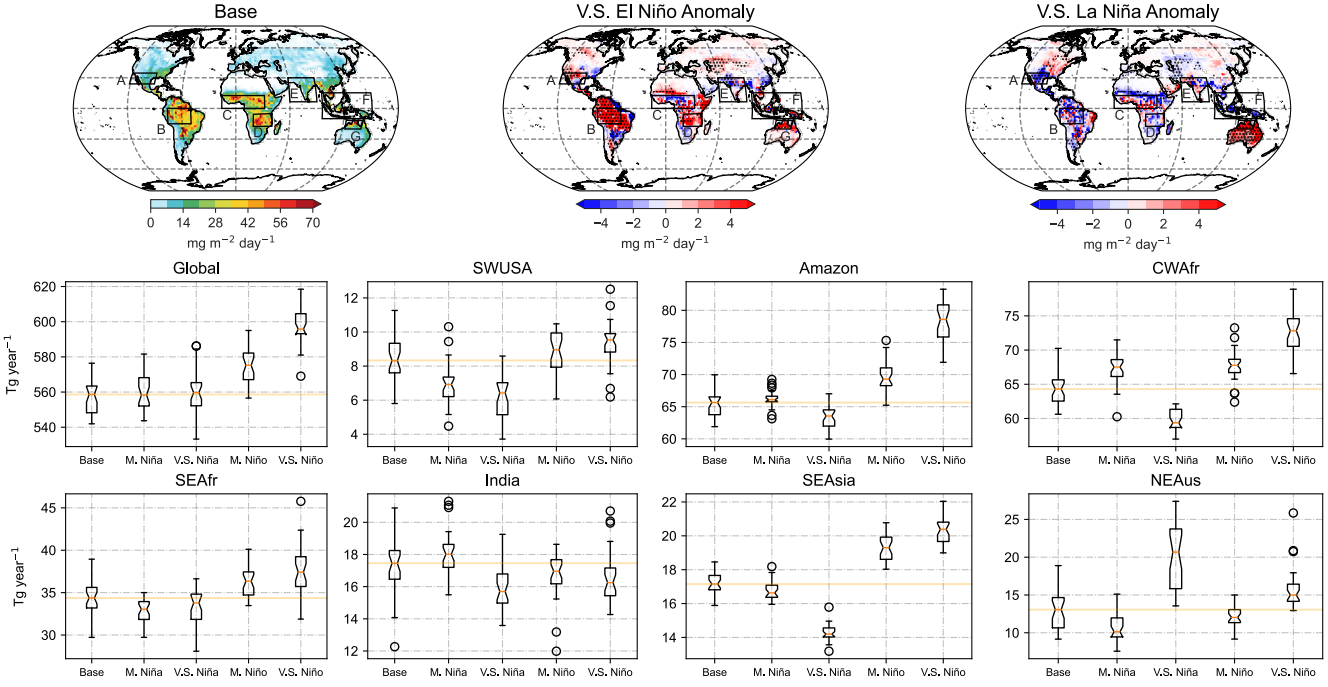

Figure 7. Global isoprene fluxes for the base scenarios as well as changes in emissions during *very strong* El Niño and La Niña events.The barplots show emission changes for the different scenarios. The median of the base scenario is indicated in orange.

Fig. 7 shows isoprene fluxes for base conditions as well as emission changes during *very strong* El Niño and La Niña scenarios averaged over thirty years. The box-whisker plots compare emission values for all scenarios over different regions. Global annual isoprene emissions in the base case are 557 Tg. Only El Niño scenarios yield a statistically significant increase in yearly emissions with 573 Tg (+ 2.87%) and 597 Tg (+ 3.95%) for *moderate* and *very strong* scenarios respectively. Over SWUSA, isoprene emissions during the base scenarios are 8.3 Tg yr^{-1} while in the *moderate* and *very strong* La Niña emissions are 7 Tg yr^{-1} (-15.66%) and 6.1 Tg yr^{-1} (-26.51%) respectively. Changes during El Niño over SWUSA are statistically insignificant. In the base scenario, emissions over the Amazon are 64.5 Tg yr^{-1}, and while anomalies during La Niña are statistically insignificant, isoprene emissions increase to 68.15 Tg yr^{-1} (+ 5.66%) and 77.35 Tg yr^{-1} (+ 19.84%) in *moderate* and *very strong* El Niño scenarios respectively. In CWAfr, anomalies are statistically significant in all scenarios. There is an increase of 2.87% and a decrease of 6.96% in *moderate* and *very strong* La Niña scenarios respectively, and an increase of 4.26%, and 11.48% in *moderate* and *very strong* El Niño scenarios respectively.

In SEAfr, statistically significant anomalies only occur in the *very strong* El Niño scenario with and increase from 34.13 Tg yr^{-1} to 38.13 Tg yr^{-1} (+ 11.72%) from base scenarios to *very strong* El Niño. Over India changes in emissions in all scenarios are statistically insignificant. Emissions from SEAsia are 16.56 Tg yr^{-1}, and while anomalies for *moderate* La Niña are not

https://doi.org/10.5194/egusphere-2023-777
Preprint. Discussion started: 3 May 2023

statistically significant, during *very strong* La Niña emissions drops to 14.99 Tg yr^{-1}, and increase to 19.22 Tg yr^{-1} and 19.92 Tg yr^{-1} during *moderate* and *very strong* El Niño scenarios respectively. Lastly, over NEAus, base emissions are 12.95 Tg yr^{-1} and increase to 20.14 Tg yr^{-1} during *very strong* La Niña, the only statistically significant anomaly. We again underline the fact that these emission changes may be exaggerated as they include long-term changes in the biosphere in this climatic mode. They could be seen as an upper range for ENSO-induced emission flux changes in this climatic mode.

Correlations between fluxes and driving variables

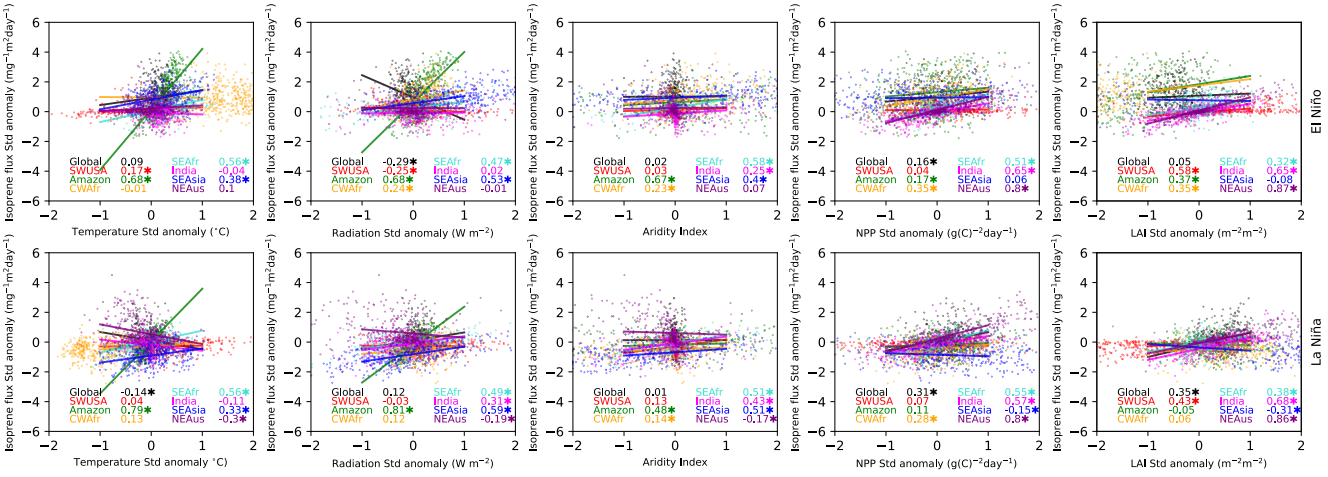

Figure 8. The Person's correlation (r) between the standardized isoprene flux anomaly and standardized temperature, radiation, AI, NPP, and LAI anomaly at different regions for *very strong* El Niño (top panels) and La Niña (bottom panels) events. Correlations with p<.01 are marked with a star.

Fig. 8 displays relationships between the standardized isoprene flux anomaly with surface temperature, radiation, and AI standardized anomalies for the different regions in climatic simulations. Surface temperatures and isoprene fluxes are generally positively correlated during El Niño. Strong correlations are found over the Amazon ($r = 0.67$), SE Africa ($r = 0.55$), and SE Asia ($r = 0.40$). All other regional and global correlations are very weak. During La Niña, there is a strong correlations between the standardized isoprene flux anomaly and temperature standardized anomaly over the Amazon ($r = 0.79$) and SE Africa ($r = 0.58$). The isoprene emissions standardized anomaly correlates well with the net solar surface radiation standardized anomaly over the Amazon ($r = 0.67$), SE fri ($r = 0.47$), and SEAsia ($r = 0.53$) during El Niño, and also during La Niña with $r = 0.81, 0.50$, and 0.60 for Amazon, SEAfr and SEAsia, respectively. The AI correlates well over the Amazon and SEAfr during El Niño. Generally, the vegetation activity (both NPP and LAI) positively correlates with isoprene emissions. In both El Niño and La Niña events, the NPP strongly correlates with isoprene fluxes over SEAfr El Niño $r = 0.51$, La Niña $r = 0.54$), India (El Niño $r = 0.66$, La Niña $r = 0.57$), and NWAus (El Niño $r = 0.80$, La Niña $r = 0.80$), while strong positive correlations with the LAI are seen over NWUSA (El Niño $r = 0.58$, La Niña $r = 0.44$), India (El Niño $r = 0.63$, La Niña $r = 0.67$), and NWAus (El Niño $r = 0.87$, La Niña $r = 0.86$).

https://doi.org/10.5194/egusphere-2023-777
Preprint. Discussion started: 3 May 2023

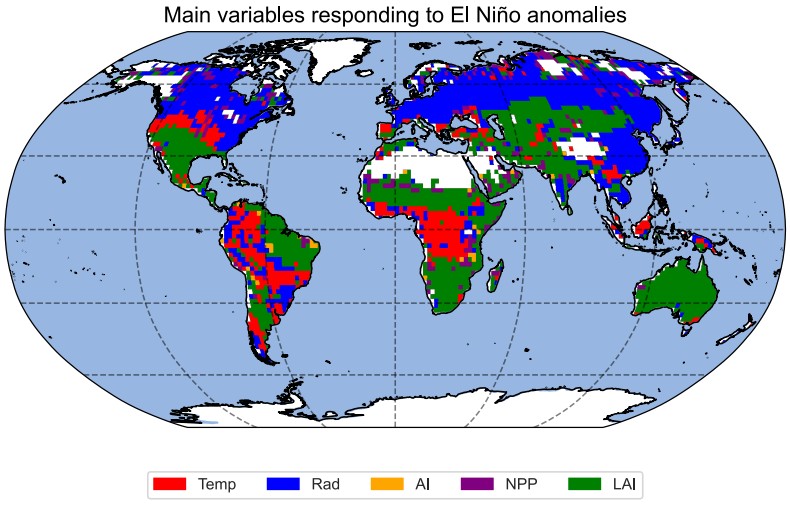

Figure 9. Map showing the variable whose anomaly correlates most strongly with the isoprene flux change for every pixel of the model output. The correlations between the isoprene flux and the temperature, radiation, AI, NPP and LAI anomalies are classified using PCA.

For each grid-cell of the model output, PCA was used to determine the variable whose ENSO anomaly correlates most strongly with the BVOC anomaly in order to find the primary cause of the variations in BVOC emission caused by ENSO. Fig. 9 shows the spatial distribution of the dominant variable that correlates most strongly with changes in isoprene fluxes. We conclude that in the northern latitudes, changes in surface radiation from ENSO correlates best with changes in isoprene emissions, suggesting that in this region isoprene fluxes are mostly influenced by surface radiation anomalies, typically linked with cloud cover and aerosol changes (Scott et al., 2018; Petäjä et al., 2022). The high dependence of BVOC fluxes on changes in surface radiation over Boreal forests indicates potential links between secondary organic aerosol (SOA) precursor emissions, cloud cover, and albedo. This model setup will be used to investigate further the aerosol-cloud-radiation interactions driven by BVOC emissions. In the tropics, especially central Africa, changes in isoprene fluxes from ENSO are mostly driven by temperature anomalies. For most of the southern USA, north east South America, South Africa, Central Asia and Australia, we find that anomalies in BVOC fluxes are likely to be driven mostly by changes in the LAI, implying that changes in vegetation can have a significant influence on the budgets of BVOC emissions.

4 Conclusions

This work sheds light on the complex interactions between atmospheric, oceanic and vegetation processes during ENSO events. Compared to previous work with historical transient simulations (or observations), we used isolated and sustained ENSO scenarios to constrain BVOC emission flux anomalies resulting from ENSO without additional natural forcing from the climate system. The isolated ENSO event simulations suggest a global increase of 2.9% in isoprene emission fluxes over two years

https://doi.org/10.5194/egusphere-2023-777
Preprint. Discussion started: 3 May 2023

with a very strong El Niño event. These simulations also show that a single ENSO event perturbs emission fluxes to the point where they do not return to baseline emissions within several years after the event.

We report potential vegetation changes as persistent ENSO condition shift the vegetation into a new quasi-equilibrium state. Over SE Asia, the fractional coverage of tropical broad-leaved evergreen trees could decreases by 8.6% and increase by 4.9% during persistent El Niño and La Niña scenarios, respectively. Our results show that if ENSO, particularly El Niño, becomes more persistent in the future we should expect an amplification in BVOC flux changes as we enter this new climatic mode with long term influence on the biosphere. In this climate mode, isoprene emissions from the Amazon could increase by 19%. We also show that ENSO-induced variations in BVOC emissions over the tropics are largely related to surface temperature anomalies, whereas surface radiation predominates at higher latitudes. Variations in the LAI were strongly linked to anomalies in BVOC emissions over the subtropics, indicating that ENSO-induced changes in plant phenology are an important driver of BVOC emissions.

Data availability. The datasets from this work will be made available on request to the corresponding author.

Author contributions. RV, AP and HT conceptualised the study and planned the experiments with significant contributions from JL. RV performed the simulations and data analysis. The results were interpreted by all co-authors, with a special focus on vegetation analysis provided by MF and TH. RV wrote the article with significant inputs from all co-authors.

Competing interests. The authors declare that they have no competing interests.

Acknowledgements. This research was conducted using the supercomputer Mogon and/or advisory services offered by Johannes Gutenberg University Mainz (https://hpc.uni-mainz.de/, last access: 4 April 2023), which is a member of the AHRP (Alliance for High Performance Computing in Rhineland Palatinate, https: //www.ahrp.info/, last access: 4 April 2023) and the Gauss Alliance e.V. This work was supported by the Max Planck Graduate Center with the Johannes Gutenberg-Universität Mainz (MPGC).

https://doi.org/10.5194/egusphere-2023-777
Preprint. Discussion started: 3 May 2023

References

Ahlström, A., Raupach, M. R., Schurgers, G., Smith, B., Arneth, A., Jung, M., Reichstein, M., Canadell, J. G., Friedlingstein, P., Jain, A. K., et al.: The dominant role of semi-arid ecosystems in the trend and variability of the land CO2 sink, Science, 348, 895–899, 2015.

Alessandri, A., Catalano, F., De Felice, M., Van Den Hurk, B., Reyes, F. D., Boussetta, S., Balsamo, G., and Miller, P. A.: Multi-scale enhancement of climate prediction over land by increasing the model sensitivity to vegetation variability in EC-Earth, Climate dynamics, 49, 1215–1237, 2017.

Arneth, A., Harrison, S. P., Zaehle, S., Tsigaridis, K., Menon, S., Bartlein, P., Feichter, J., Korhola, A., Kulmala, M., O'donnell, D., et al.: Terrestrial biogeochemical feedbacks in the climate system, Nature Geoscience, 3, 525–532, 2010.

Atkinson, R.: Atmospheric chemistry of VOCs and NOx, Atmospheric environment, 34, 2063–2101, 2000.

Atkinson, R. and Arey, J.: Gas-phase tropospheric chemistry of biogenic volatile organic compounds: a review, Atmospheric Environment, 37, 197–219, 2003.

Bacer, S., Christoudias, T., and Pozzer, A.: Projection of North Atlantic Oscillation and its effect on tracer transport, Atmospheric Chemistry and Physics, 16, 15 581–15 592, 2016.

Bastos, A., Friedlingstein, P., Sitch, S., Chen, C., Mialon, A., Wigneron, J.-P., Arora, V. K., Briggs, P. R., Canadell, J. G., Ciais, P., et al.: Impact of the 2015/2016 El Niño on the terrestrial carbon cycle constrained by bottom-up and top-down approaches, Philosophical Transactions of the Royal Society B: Biological Sciences, 373, 20170 304, 2018.

Cai, W., Santoso, A., Wang, G., Yeh, S.-W., An, S.-I., Cobb, K. M., Collins, M., Guilyardi, E., Jin, F.-F., Kug, J.-S., et al.: ENSO and greenhouse warming, Nature Climate Change, 5, 849–859, 2015.

Chang, J., Ciais, P., Wang, X., Piao, S., Asrar, G., Betts, R., Chevallier, F., Dury, M., François, L., Frieler, K., et al.: Benchmarking carbon fluxes of the ISIMIP2a biome models, Environmental Research Letters, 12, 045 002, 2017.

Dai, A. and Wigley, T.: Global patterns of ENSO-induced precipitation, Geophysical Research Letters, 27, 1283–1286, 2000.

Ehn, M., Thornton, J. A., Kleist, E., Sipilä, M., Junninen, H., Pullinen, I., Springer, M., Rubach, F., Tillmann, R., Lee, B., et al.: A large source of low-volatility secondary organic aerosol, Nature, 506, 476–479, 2014.

Forrest, M., Tost, H., Lelieveld, J., and Hickler, T.: Including vegetation dynamics in an atmospheric chemistry-enabled general circulation model: linking LPJ-GUESS (v4. 0) with the EMAC modelling system (v2. 53), Geoscientific Model Development, 13, 1285–1309, 2020.

Gong, D. and Wang, S.: Impacts of ENSO on rainfall of global land and China, Chinese Science Bulletin, 44, 852–857, 1999.

Gonsamo, A., Chen, J. M., and Lombardozzi, D.: Global vegetation productivity response to climatic oscillations during the satellite era, Global change biology, 22, 3414–3426, 2016.

Guenther, A., Hewitt, C. N., Erickson, D., Fall, R., Geron, C., Graedel, T., Harley, P., Klinger, L., Lerdau, M., McKay, W., et al.: A global model of natural volatile organic compound emissions, Journal of Geophysical Research: Atmospheres, 100, 8873–8892, 1995.

Guenther, A., Karl, T., Harley, P., Wiedinmyer, C., Palmer, P. I., and Geron, C.: Estimates of global terrestrial isoprene emissions using MEGAN (Model of Emissions of Gases and Aerosols from Nature), Atmospheric Chemistry and Physics, 6, 3181–3210, 2006.

Guenther, A. B., Zimmerman, P. R., Harley, P. C., Monson, R. K., and Fall, R.: Isoprene and monoterpene emission rate variability: model evaluations and sensitivity analyses, Journal of Geophysical Research: Atmospheres, 98, 12 609–12 617, 1993.

Jöckel, P., Sander, R., Kerkweg, A., Tost, H., and Lelieveld, J.: the modular earth submodel system (MESSy)-a new approach towards earth system modeling, Atmospheric Chemistry and Physics, 5, 433–444, 2005.

https://doi.org/10.5194/egusphere-2023-777
Preprint. Discussion started: 3 May 2023

Jöckel, P., Tost, H., Pozzer, A., Kunze, M., Kirner, O., Brenninkmeijer, C. A., Brinkop, S., Cai, D. S., Dyroff, C., Eckstein, J., et al.: Earth system chemistry integrated modelling (ESCiMo) with the modular earth submodel system (MESSy) version 2.51, Geoscientific Model Development, 9, 1153–1200, 2016.

Karl, T., Harley, P., Emmons, L., Thornton, B., Guenther, A., Basu, C., Turnipseed, A., and Jardine, K.: Efficient atmospheric cleansing of oxidized organic trace gases by vegetation, Science, 330, 816–819, 2010.

Kerkweg, A., Sander, R., Tost, H., and Jöckel, P.: Implementation of prescribed (OFFLEM), calculated (ONLEM), and pseudo-emissions (TNUDGE) of chemical species in the Modular Earth Submodel System (MESSy), Atmospheric Chemistry and Physics, 6, 3603–3609, 2006.

Laothawornkitkul, J., Paul, N. D., Vickers, C. E., Possell, M., Taylor, J. E., Mullineaux, P. M., and Hewitt, C. N.: Isoprene emissions influence herbivore feeding decisions, Plant, cell & environment, 31, 1410–1415, 2008.

Lathiere, J., Hauglustaine, D., Friend, A., Noblet-Ducoudré, D., Viovy, N., Folberth, G., et al.: Impact of climate variability and land use changes on global biogenic volatile organic compound emissions, Atmospheric Chemistry and Physics, 6, 2129–2146, 2006.

Lee, J.-Y., Marotzke, J., Bala, G., Cao, L., Corti, S., Dunne, J. P., Engelbrecht, F., Fischer, E., Fyfe, J. C., Jones, C., et al.: Future global climate: scenario-based projections and near-term information, IPCC, 2021.

McPhaden, M. J., Zebiak, S. E., and Glantz, M. H.: ENSO as an integrating concept in earth science, science, 314, 1740–1745, 2006.

Müller, J.-F., Stavrakou, T., Wallens, S., De Smedt, I., Van Roozendael, M., Potosnak, M., Rinne, J., Munger, B., Goldstein, A., and Guenther, A.: Global isoprene emissions estimated using MEGAN, ECMWF analyses and a detailed canopy environment model, Atmospheric Chemistry and Physics, 8, 1329–1341, 2008.

Nemani, R. R., Keeling, C. D., Hashimoto, H., Jolly, W. M., Piper, S. C., Tucker, C. J., Myneni, R. B., and Running, S. W.: Climate-driven increases in global terrestrial net primary production from 1982 to 1999, science, 300, 1560–1563, 2003.

Palm, B. B., de Sá, S. S., Day, D. A., Campuzano-Jost, P., Hu, W., Seco, R., Sjostedt, S. J., Park, J.-H., Guenther, A. B., Kim, S., et al.: Secondary organic aerosol formation from ambient air in an oxidation flow reactor in central Amazonia, Atmospheric Chemistry and Physics, 18, 467–493, 2018.

Peñuelas, J. and Staudt, M.: BVOCs and global change, Trends in plant science, 15, 133–144, 2010.

Petäjä, T., Tabakova, K., Manninen, A., Ezhova, E., O'Connor, E., Moisseev, D., Sinclair, V. A., Backman, J., Levula, J., Luoma, K., et al.: Influence of biogenic emissions from boreal forests on aerosol–cloud interactions, Nature Geoscience, 15, 42–47, 2022.

Pöschl, U., Martin, S., Sinha, B., Chen, Q., Gunthe, S., Huffman, J., Borrmann, S., Farmer, D., Garland, R., Helas, G., et al.: Rainforest aerosols as biogenic nuclei of clouds and precipitation in the Amazon, science, 329, 1513–1516, 2010.

Roeckner, E., Brokopf, R., Esch, M., Giorgetta, M., Hagemann, S., Kornblueh, L., Manzini, E., Schlese, U., and Schulzweida, U.: Sensitivity of simulated climate to horizontal and vertical resolution in the ECHAM5 atmosphere model, Journal of Climate, 19, 3771–3791, 2006.

Ropelewski, C. F. and Halpert, M. S.: North American precipitation and temperature patterns associated with the El Niño/Southern Oscillation (ENSO), Monthly Weather Review, 114, 2352–2362, 1986.

Scott, C., Arnold, S., Monks, S., Asmi, A., Paasonen, P., and Spracklen, D.: Substantial large-scale feedbacks between natural aerosols and climate, Nature Geoscience, 11, 44–48, 2018.

Sharkey, T. D. and Loreto, F.: Water stress, temperature, and light effects on the capacity for isoprene emission and photosynthesis of kudzu leaves, Oecologia, 95, 328–333, 1993.

Sharkey, T. D. and Monson, R. K.: Isoprene research–60 years later, the biology is still enigmatic, Plant, cell & environment, 40, 1671–1678, 2017.

https://doi.org/10.5194/egusphere-2023-777
Preprint. Discussion started: 3 May 2023

Smith, B., Prentice, I. C., and Sykes, M. T.: Representation of vegetation dynamics in the modelling of terrestrial ecosystems: comparing two contrasting approaches within European climate space, Global ecology and biogeography, pp. 621–637, 2001.

Smith, B., Wårlind, D., Arneth, A., Hickler, T., Leadley, P., Siltberg, J., and Zaehle, S.: Implications of incorporating N cycling and N limitations on primary production in an individual-based dynamic vegetation model, Biogeosciences, 11, 2027–2054, 2014.

Teckentrup, L., De Kauwe, M. G., Pitman, A. J., and Smith, B.: Examining the sensitivity of the terrestrial carbon cycle to the expression of El Niño, Biogeosciences, 18, 2181–2203, 2021.

Tost, H.: Chemistry–climate interactions of aerosol nitrate from lightning, Atmospheric Chemistry and Physics, 17, 1125–1142, 2017.

Vella, R., Forrest, M., Lelieveld, J., and Tost, H.: Isoprene and monoterpene simulations using the chemistry-climate model EMAC (v2.55) with interactive vegetation from LPJ-GUESS (v4.0), Geoscientific Model Development, 16, 885–906, 2023.

Vickers, C. E., Gershenzon, J., Lerdau, M. T., and Loreto, F.: A unified mechanism of action for volatile isoprenoids in plant abiotic stress, Nature chemical biology, 5, 283–291, 2009.

Wang, J., Zeng, N., Wang, M., Jiang, F., Wang, H., and Jiang, Z.: Contrasting terrestrial carbon cycle responses to the 1997/98 and 2015/16 extreme El Niño events, Earth System Dynamics, 9, 1–14, 2018.

Weiss, M., Miller, P. A., van den Hurk, B. J., van Noije, T., Ştefănescu, S., Haarsma, R., Van Ulft, L. H., Hazeleger, W., Le Sager, P., Smith, B., et al.: Contribution of dynamic vegetation phenology to decadal climate predictability, Journal of Climate, 27, 8563–8577, 2014.

Wells, K. C., Millet, D. B., Payne, V. H., Deventer, M. J., Bates, K. H., de Gouw, J. A., Graus, M., Warneke, C., Wisthaler, A., and Fuentes, J. D.: Satellite isoprene retrievals constrain emissions and atmospheric oxidation, Nature, 585, 225–233, 2020.

Wu, R., Hu, Z.-Z., and Kirtman, B. P.: Evolution of ENSO-related rainfall anomalies in East Asia, Journal of Climate, 16, 3742–3758, 2003.

Zhang, Y., Dannenberg, M. P., Hwang, T., and Song, C.: El Niño-Southern Oscillation-induced variability of terrestrial gross primary production during the satellite era, Journal of Geophysical Research: Biogeosciences, 124, 2419–2431, 2019.

Zhu, Z., Piao, S., Xu, Y., Bastos, A., Ciais, P., and Peng, S.: The effects of teleconnections on carbon fluxes of global terrestrial ecosystems, Geophysical Research Letters, 44, 3209–3218, 2017.

Zuo, Z., Weraduwage, S. M., Lantz, A. T., Sanchez, L. M., Weise, S. E., Wang, J., Childs, K. L., and Sharkey, T. D.: Isoprene acts as a signaling molecule in gene networks important for stress responses and plant growth, Plant Physiology, 180, 124–152, 2019.